JACS
JOURNAL OF THE AMERICAN CHEMICAL SOCIETY

ARTICLE

pubs.acs.org/JACS

Bionano Donor–Acceptor Hybrids of Porphyrin, ssDNA, and Semiconductive Single-Wall Carbon Nanotubes for Electron Transfer via Porphyrin Excitation

Francis D'Souza,*[,†,‡] Sushanta K. Das,[†] Melvin E. Zandler,[‡] Atula S. D. Sandanayaka,[§] and Osamu Ito*[,∥]

[†]Contribution from the Department of Chemistry, University of North Texas, 1155 Union Circle, #305070, Denton, Texas 76203-5017, United States

[‡]Department of Chemistry, Wichita State University, 1845 Fairmount, Wichita, Kansas 67260-0051, United States

[§]School of Materials Science, Japan Advanced Institute of Science and Technology (JAIST), Nomi, Ishikawa, 923-1292 Japan

[∥]CarbonPhotoScience Lab., Kita-Nakayama 2-1-6, Izumi-ku, Sendai, 981-3215 Japan

Supporting Information

ABSTRACT: Photoinduced electron transfer in self-assemblies of porphyrins ion-paired with ssDNA wrapped around single-wall carbon nanotubes (SWCNTs) has been reported. To accomplish the three-component hybrids, two kinds of diameter-sorted semiconducting SWCNT(*n*,*m*)s of different diameter ((*n*,*m*) = (6,5) and (7,6)) and free-base or zinc porphyrin bearing peripheral positive charges ((TMPyP$^+$)M (tetrakis(4-*N*-methylpyridyl)porphyrin); M = Zn and H_2) serving as light-absorbing photoactive materials are utilized. The donor–acceptor hybrids are held by ion-pairing between the negatively charged phosphate groups of ssDNA on the surface of the SWCNT and the positively charged at the ring periphery porphyrin macrocycle. The newly assembled bionano donor–acceptor hybrids have been characterized by transmission electron microscopy (TEM) and spectroscopic methods. Photoinduced electron transfer from the excited singlet porphyrin to the SWCNTs directly and/or via ssDNA as an electron mediator has been established by performing systematic studies involving the steady-state and time-resolved emission as well as the transient absorption studies. Higher charge-separation efficiency has been successfully demonstrated by the selection of the appropriate semiconductive SWCNTs with the right band gap, in addition to the aid of ssDNA as the electron mediator.

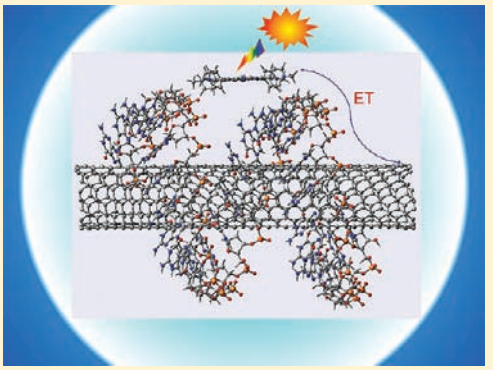

INTRODUCTION

Recently, DNA[1]–single-wall carbon nanotube (SWCNT)[2−4] bionano hybrids have witnessed a variety of nanotechnological applications including chemical and biomolecular sensing and devices,[5] exfoliation and sorting of SWCNTs,[6] and ultrafast DNA sequencing.[7] However, although SWCNTs have been demonstrated to be both good electron donors and electron acceptors in the presence of appropriate photosensitizing electron acceptors or donors, respectively,[8−11] utilization of DNA–SWCNT hybrids in electron-transfer reactions has not been exploited. In the present investigation, we have undertaken this mission to reveal the applicability of DNA–SWCNT bionano hybrids for the light-energy harvesting photoinduced electron transfer devices.

The bionano donor–acceptor hybrids are formed by wrapping ssDNA around the SWCNTs and by ion-pairing water-soluble cationic porphyrins to the phosphate groups of ssDNA strands (see Figure 1 for a schematic structure). To obtain the structure–reactivity aspects, two types of diameter-sorted SWCNTs such as SWCNT(6,5) and SWCNT(7,6) differing in their oxidation and reduction potentials have been employed as donor–acceptor nanocarbons.[12] We have chosen ssDNA in the present study since the SWCNT hybrids with this biomolecule are one of the

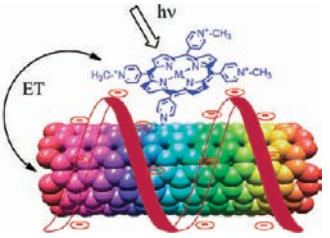

Figure 1. Schematic presentation of the constructed bionano donor–acceptor hybrids, (TMPyP$^+$)M/ssDNA/SWCNT(*n*,*m*) {TMPyP$^+$ = tetrakis(*N*-methylpyridyl)porphyrin, M = Zn or H_2; (*n*,*m*) = (6,5) or (7,6)}, formed by a combination of ssDNA wrapping and ion-pairing binding protocols. The tape structure represents ssDNA wrapped around SWCNTs, and the negative sign indicates phosphate groups.

well-characterized bionano hybrids with two-layered structures (ssDNA/SWCNT(*n*,*m*)). The atomic force microscopy (AFM),[13] transmission electron microscopy (TEM),[13] circular dichroism,[14] and computational modeling studies[15] have demonstrated

Received: September 5, 2011
Published: November 16, 2011

dx.doi.org/10.1021/ja208380b | *J. Am. Chem. Soc.* 2011, 133, 19922–19930

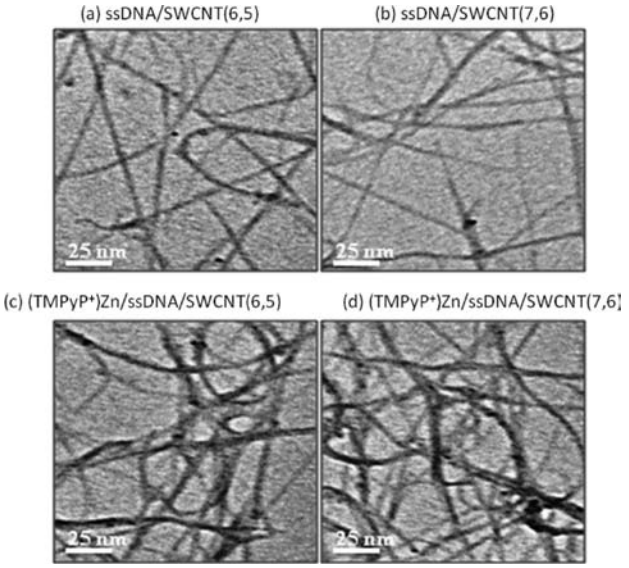

Figure 2. TEM images of (a) ssDNA/SWCNT(6,5), (b) ssDNA/SWCNT(7,6), (c) $(TMPyP^+)$Zn/ssDNA/SWCNT(6,5), and (d) $(TMPyP^+)$Zn/ssDNA/SWCNT(7,6).

exfoliation and helical wrapping of ssDNA around the side walls of SWCNTs. As light-absorbing photoactive materials,[16] free-base and zinc porphyrins bearing peripheral positive charges (tetrakis-(4-*N*-methylpyridyl)porphyrin abbreviated as $(TMPyP^+)$M, M = H_2 and Zn) are utilized. By the addition of $(TMPyP^+)$M to ssDNA/SWCNT(*n,m*), $(TMPyP^+)$M can be attached to the ssDNA wrapped around SWCNT(*n,m*) by ion-pairing binding, forming three-layered structures ($(TMPyP^+)$M/ssDNA/SWCNT(*n,m*)). In the present study, photochemical and photophysical studies leading to charge separation in the newly assembled bionano donor–acceptor hybrids have been established using various steady-state spectroscopic and transient spectral measurements, expecting that the ssDNA acts as an electron mediator for the electron transfer from the light-excited $(TMPyP^+)$M to SWCNT. Furthermore, by the selection of the appropriate semiconductive SWCNTs of the right band gap and also selection of M = H_2 and Zn in $(TMPyP^+)$M, the possibility of achieving higher charge-separation efficiency is demonstrated.

RESULTS AND DISCUSSION

The enriched SWCNT(6,5) and SWCNT(7,6) samples employed in the present study have an average radius of 8 and 9 Å, respectively, with an average length of 800 nm.[17,18] The preparations of the two-layered ssDNA/SWCNT(*n,m*) were performed by adding ssDNA to SWCNT(*n,m*) dispersed in water, resulting into homogeneous solution after sonication. Then, the three-layered supramolecules $(TMPyP^+)$M/ssDNA/SWCNT(*n,m*)s were obtained by adding $(TMPyP^+)$M to ssDNA/SWCNT(*n,m*) in H_2O. Details are given in the Experimental Section. From the weight of the individual components used in the formation of nanohybrids and their absorbance (ε) values, one porphyrin molecule for every 25–30 nm length of ssDNA/SWCNT, which corresponds to 18–24 porphyrins for single ssDNA/SWCNT of 800 nm length, was estimated.[19]

TEM Images. TEM images for the dried samples of ssDNA/SWCNT(*n,m*) and $(TMPyP^+)$Zn/ssDNA/SWCNT(*n,m*) are shown in Figure 2; similar TEM images were obtained for

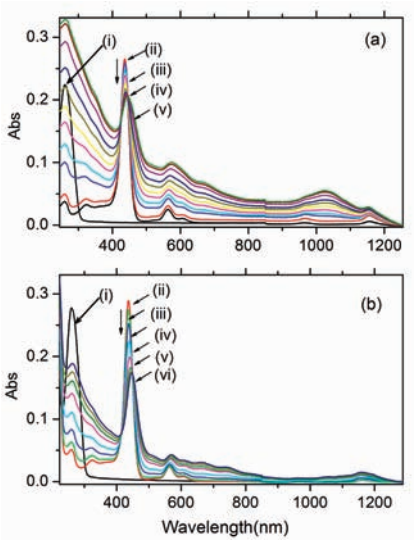

Figure 3. Steady-state absorption spectral changes of (i) ssDNA and (ii) $(TMPyP^+)$Zn; (a) SWCNT(6,5) and (b) SWCNT(7,6), on addition of ssDNA/SWCNT(*n,m*) to $(TMPyP^+)$ in H_2O; (iii)–(vi) spectrum of $(TMPyP^+)$Zn on increasing addition of ssDNA/SWCNT(6,5). (Note: Concentration change of porphyrin on addition of ssDNA stock solution with volume increase was minor compared with the absorbance decrease.)

$(TMPyP^+)H_2$/ssDNA/SWCNT(*n,m*) (see Supporting Information, Figure S1). The images of ssDNA/SWCNT(*n,m*) in Figures 2a and 2b show that the nanotubes are in a sufficiently exfoliated state, suggesting that ssDNA disperses bundles of SWCNT(*n,m*) by forming two-layered supramolecular ssDNA/SWCNT(*n,m*) hybrids in H_2O. However, as shown in Figures 2c and 2d for $(TMPyP^+)$Zn/ssDNA/SWCNT(*n,m*), the TEM images and the histograms in Figure S2 (Supporting Information) revealed increased thickness with higher tangles of SWCNTs. This suggests binding of the $(TMPyP^+)$Zn molecules to ssDNA/SWCNT(*n,m*) thus increasing the radii, in addition to the $(TMPyP^+)$Zn molecules intertwining several ssDNA/SWCNT-(*n,m*) tubes.

Steady-State Absorption Spectral Studies. One of the advantages of obtaining homogeneous dispersion of the $(TMPyP^+)$-Zn/ssDNA/SWCNT(*n,m*) nanohybrids is the ability of measuring their various spectroscopic properties, which provide fundamental features of the SWCNT(*n,m*) nanohybrids in solution. Steady-state absorption spectra of SWCNT(*n,m*) dispersed in ssDNA and in sodium dodecyl sulfate (SDS) surfactant are shown in Figure S3 in the Supporting Information. The absorption spectrum of SWCNT(6,5) in the presence of ssDNA shows the longest absorption peak of SWCNT(6,5) at 1007 nm resulting in a band gap of 1.23 eV, in addition to the 261 nm band of ssDNA. Compared with the sharp absorption peak (977 nm = 1.26 eV) of SWCNT(6,5) dispersed in SDS surfactant, a red shift with broadening was caused by the ssDNA surrounding, resulting in band gap narrowing of 0.03 eV.[20,21] For SWCNT(7,6), the longest absorption peak in the presence of ssDNA is located at 1200 nm, giving a band gap of 1.03 eV, which also shows a band gap narrowing compared with that in less interacting SDS solution (1122 nm = 1.10 eV) by 0.07 eV.[20,21] These appreciable red-shifts in the absorption peaks and broadening on addition of ssDNA to SWCNT(*n,m*) support the formation of ssDNA/SWCNT(*n,m*).

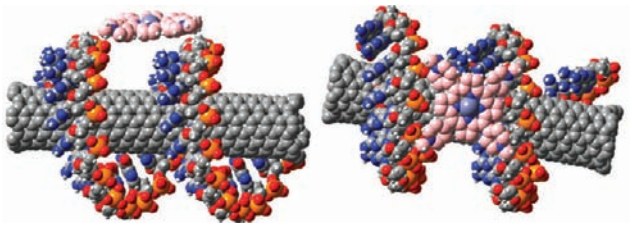

Figure 4. PM3 optimized structure of $(TMPyP^+)Zn$/ssDNA/SWCNT-(7,6) from different viewpoints. For ssDNA/SWCNT(7,6): C, gray; H, white; N, blue; O, red; P, orange. For $(TMPyP^+)Zn$, colors are coded differently for easy recognition: C, pink; H, white; N, blue; Zn, light blue. (Left): Side view with respect to $(TMPyP^+)Zn$. (Right): Top view with respect to $(TMPyP^+)Zn$, in which there is a space about 6 Å between the surfaces of $(TMPyP^+)Zn$ and SWCNT(7,6).

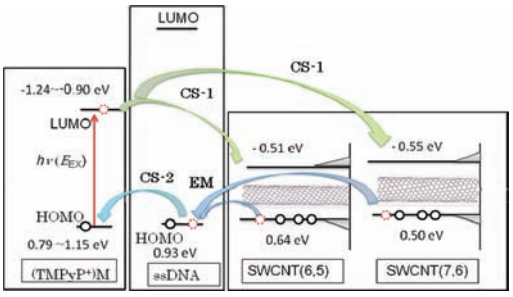

Figure 5. Schematic representation of the energy level diagram for photoinduced electron transfer processes of $(TMPyP^+)M$/ssDNA/SWCNT(n,m) (M = Zn and H_2, and (n,m) = (6,5) and (7,6)); electron denoted as a red dotted circle is a moving electron.

The sensitizer, $(TMPyP^+)Zn$, shows the Soret band at 425 nm and Q bands at 560 and 605 nm in H_2O.[13] On addition of ssDNA to $(TMPyP^+)Zn$, the Soret band at 425 nm shifted to longer wavelength accompanied by a decrease in the peak intensity, suggesting the formation of $(TMPyP^+)Zn$/ssDNA (see Figure S4 in the Supporting Information).

Figure 3 shows absorption spectral changes of $(TMPyP^+)Zn$ on addition of ssDNA/SWCNT(n,m). In Figure 3a for SWNCT(6,5), the Soret band at 425 nm of $(TMPyP^+)Zn$ shifts to longer wavelength with a significant decrease in the absorption band intensity, even though the other absorption intensities increase in a whole UV−vis−NIR region due to ssDNA/SWNCT(6,5). Such absorption spectral changes at the Soret band are caused by the interaction of the porphyrin moiety with ssDNA, supporting the formation of $(TMPyP^+)Zn$/ssDNA/SWCNT(6,5). Similar absorption spectral changes were observed on addition of ssDNA/SWCNT(7,6) to $(TMPyP^+)Zn$ as shown in Figure 3b, in which the decrease of the absorption band intensity with an appreciable red-shift and band broadening of $(TMPyP^+)Zn$ was observed, in spite of the increasing intensities in the whole spectral region of ssDNA/SWNCT(7,6). Similar spectral changes were observed for $(TMPyP^+)H_2$ on addition of ssDNA/SWNCT(n,m). It may be mentioned here that direct interactions between $(TMPyP^+)M$ and SWCNT (through weak $\pi-\pi$ interactions) may be excluded since the ion-pairing interactions involving ssDNA and porphyrin are much stronger, and also the interactions between ssDNA wrapped around SWCNT may also be strong enough not to be replaced with $(TMPyP^+)M$.

Energy Optimization Structure. An attempt was also made to visualize the structure of the donor−acceptor bionano hybrids using the energy optimization calculation method. Figure 4 shows the PM3-optimized structure of $(TMPyP^+)Zn$/ssDNA/SWCNT(7,6) as an example, in which the stabilized structure of ssDNA/SWCNT(7,6) by wrapping of ssDNA around the nanotube is clearly seen.[22] Additionally, $(TMPyP^+)Zn$ is stabilized on the phosphate groups (orange balls) along ssDNA strands due to the ion-pairing interactions. The distance between the porphyrin plane and nanotube surface was found to be about 8 Å, a suitable distance for donor−acceptor pairs to establish efficient photoinduced formation of the charge-separated radical ion pair with long lifetime.[11] Although the distance between the porphyrin plane and ssDNA outer sphere was found to be close, the distance to the DNA bases may be slightly longer (see distance from blue balls of N-atoms).

Energy Diagrams. An energy level diagram depicting different photochemical events of the nanohybrids has been constructed using the optical data in conjunction with the reported electrochemical data.[12,23] For $(TMPyP^+)M$, the reported oxidation potentials (E_{OX}) are employed to calculate the HOMO levels (E_{HOMO}): E_{OX} = 0.79 V for $(TMPyP^+)Zn$ and 1.15 V for $(TMPyP^+)H_2$, vs Ag/AgCl in DMF.[13,19,24] The LUMO levels (E_{LUMO}) of $(TMPyP^+)M$ are evaluated from the E_{HOMO} values and the energies of the singlet excited states ($^1[(TMPyP^+)M]^*$; E_{EX} = 2.03 and 2.05 eV for M = Zn and H_2, respectively) since any reliable E_{RED} value is not reported even in DMF. Cyclic voltammetric studies of ssDNA in H_2O in the presence of 0.1 M KCl revealed an oxidation peak, E_{pc}, around 0.93 V vs Ag/AgCl that could be ascribed mainly to the oxidation of the guanidine base units.[25] In the case of SWCNT(n,m), the reported E_{OX} and E_{RED} values correspond to the highest level of the valence band and the lowest level of the conduction band.[12,13] The energy diagram combined for both $(TMPyP^+)M$ (M = Zn and H_2) is shown in Figure 5 (for each porphyrin, see Figure S5, Supporting Information).

After photoexcitation of $(TMPyP^+)M$, an electron of the HOMO is elevated to the LUMO. Then, the electron can transfer from the half-filled LUMO of $(TMPyP^+)M$ to the conduction band level of SWCNT overshooting the ssDNA layer, giving the radical cation of $(TMPyP^+)M$ ($[(TMPyP^+)M]^{\bullet+}$) and the radical anion of SWCNT(n,m) ($[SWCNT(n,m)]^{\bullet-}$), denoted as the CS-1 process in Figure 5. When the E_{ox} value of $(TMPyP^+)M$ is lower than that of ssDNA, the HOMO electron of ssDNA can transfer to the half-vacant HOMO of $(TMPyP^+)M$ after the photoexcitation, giving $[(TMPyP^+)M]^{\bullet-}$ and $[ssDNA]^{\bullet+}$, which is denoted to be the CS-2 process. After the CS-2 process, an electron can mediate from the valence-band level of SWCNT(n,m) to the half-vacant HOMO of ssDNA, which is denoted to be the electron mediation (EM) process, finally giving $[(TMPyP^+)M]^{\bullet-}$ and hole on SWCNT(n,m) ($[SWCNT(n,m)]^{\bullet+}$).

After photoexcitation of $(TMPyP^+)M$, energy transfer (EnT) from $(TMPyP^+)M$ to SWCNT(n,m) is also possible via an electron exchange between the half-vacant HOMO of $(TMPyP^+)M$ and the valence band of SWCNT(n,m).[26] However, it is difficult to promote energy transfer over the ssDNA since such a Dexter-type EnT process is only predominant in short distance exchange coupled donor−acceptor systems.[26b]

The radical ion-pair (RIP) energy for the CS-1 process ($E_{RIP(CS\text{-}1)} = E_{RIP(MP^{\bullet+})/(SWCNT^{\bullet-})}$; here, $(TMPyP^+)M$ is abbreviated as MP) can be evaluated using Weller's approach[27] as the difference between E_{OX} of $(TMPyP^+)M$ and E_{RED} of SWCNT(n,m) as listed in the margin of Table 1. The RIP energy for CS-2 ($E_{RIP(CS\text{-}2)} = E_{RIP(MP^{\bullet-})/(DNA^{\bullet+})}$) can be evaluated as the difference

Table 1. Estimated Energy Parameters for Donor−Acceptor Nanohybrids in H_2O[a]

nanohybrids	$E_{RIP(CS-1)}$	ΔG_{CS-1}	$E_{RIP(CS-2)}$	ΔG_{CS-2}	ΔG_{EM}	$\Delta G_{CS-2/EM}$	$E_{RIP(CS-2/EM)}$
$(TMPyP^+)Zn$/ssDNA/SWCNT(6,5)	1.30	−0.70	2.17	0.14	(−0.29)[b]	(−0.15)[b]	(1.88)[b]
$(TMPyP^+)Zn$/ssDNA/SWCNT(7,6)	1.34	−0.66	2.17	0.14	(−0.43)[b]	(−0.29)[b]	(1.74)[b]
$(TMPyP^+)H_2$/ssDNA/SWCNT(6,5)	1.51	−0.49	1.83	−0.22	−0.29	−0.51	1.54
$(TMPyP^+)H_2$/ssDNA/SWCNT(7,6)	1.55	−0.45	1.83	−0.22	−0.43	−0.65	1.45

[a] For $(TMPyP^+)M$, redox potentials reported in DMF are employed; E_{OX} = 0.79 and 1.15 V vs Ag/AgCl for M = Zn and H_2. The E_{RED} values are evaluated from the E_{HOMO} values; $E_{LUMO} = E_{HOMO} + E_{EX}$; $E_{HOMO} = E_{OX}$, and E_{EX} = 2.03 and 2.05 eV for M = Zn and H_2. E_{RED} = −1.24 and −0.90 V vs Ag/AgCl for M = Zn and H_2. For SWCNT(6,5), E_{OX} = 0.64 and E_{RED} = −0.51 V, and for SWCNT(7,6), E_{OX} = 0.50 and E_{RED} = −0.55 V vs Ag/AgCl in DMF.[12] E_{RIP}, ΔG_{CS}, and ΔG_{EM} are calculated according to the Weller approach assuming that the Columbic term is negligibly small.[27] [b] Assuming that the CS-2 process took place.

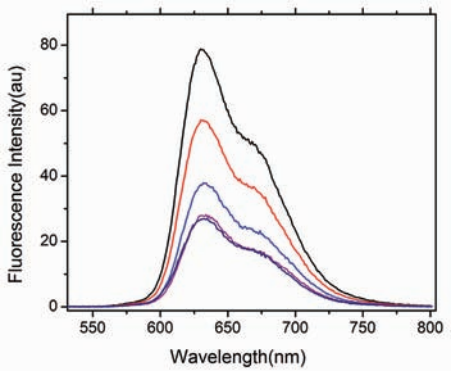

Figure 6. Steady-state fluorescence spectral changes of $(TMPyP^+)Zn$ (10 μM) on addition of ssDNA in H_2O (λ_{ex} = 435 nm). Black line is for $(TMPyP^+)Zn$ in the absence of ssDNA; red, blue, dark red, and dark blue lines are on increasing addition of ssDNA. (Note: Concentration change of porphyrin on addition of ssDNA stock solution with volume increase was minor compared with the fluorescence decrease.)

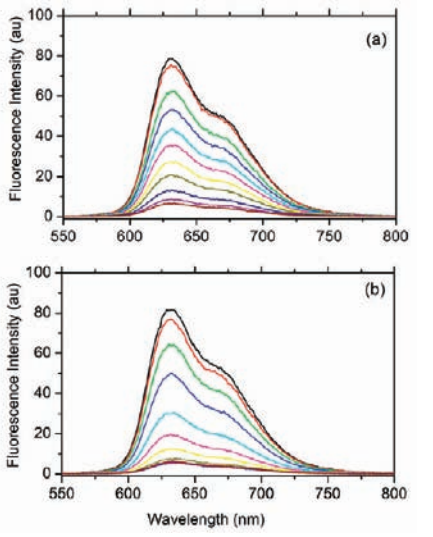

Figure 7. Steady-state fluorescence spectral changes of $(TMPyP^+)Zn$ (10 μM) on addition of (a) ssDNA/SWCNT(6,5) and (b) ssDNA/SWCNT(7,6) in H_2O (λ_{ex} = 435 nm). Black line for $(TMPyP^+)M$; red, green, blue, sky, violet, yellow, dark green, dark blue, violet, and brown lines are on increasing addition of ssDNA/SWCNT(n,m).

between E_{OX} of MP and E_{RED} of ssDNA. The RIP energy ($E_{RIP(MP^{\bullet-})/(SWCNT^{\bullet+})}$), which is the sum of $E_{RIP(CS-2)}$ and $E_{RIP(EM)}$ as denoted to be $E_{RIP(CS-2/EM)}$ in Table 1, can be evaluated from the difference between E_{RED} of $(TMPyP^+)M$ and E_{OX} of SWCNT(n,m). Thus, the free-energy changes for the CS-1 process (ΔG_{CS-1}) via $^1[(TMPyP^+)M]^*$ can be evaluated (Table 1); the negative values for ΔG_{CS-1} indicate that the CS-1 process for all systems is sufficiently exothermic. The CS-2 process for $(TMPyP^+)H_2$ is exothermic, whereas for $(TMPyP^+)Zn$, this process is slightly endothermic. These thermodynamic data predict that the CS-1 process takes priority over the CS-2 process. Since the ΔG_{EM} values are all negative predicting exothermic reactions, the overall CS-2/EM process generating $[(TMPyP^+)M]^{\bullet-}/[SWCNT]^{\bullet+}$ via $^1[(TMPyP^+)M]^*$ also becomes exothermic.

The CS-1 process for $(TMPyP^+)Zn$ with higher electron-donor ability is more exothermic than that for $(TMPyP^+)H_2$. The higher electron-acceptor capability for SWCNT(6,5) than SWCNT(7,6) prevails the exothermic CS-1 process for SWCNT(6,5). In the case of $(TMPyP^+)H_2$, the CS-2/EM for SWCNT(7,6) is slightly more exothermic than that for SWCNT(6,5).

For the charge-recombination (CR-1) process of RIP ($[(TMPyP^+)M]^{\bullet+}/[SWCNT]^{\bullet-}$), although higher exothermic CR is predicted for $(TMPyP^+)H_2$ than $(TMPyP^+)Zn$, a faster CR-1 process is not always predicted for $(TMPyP^+)H_2$ because of the inverted region in the Marcus plot.[28] The CR-1 process from $[(TMPyP^+)M]^{\bullet+}/[SWCNT]^{\bullet-}$ is predicted to be slightly more exothermic for SWCNT(7,6) than that for SWCNT(6,5), whereas an opposite tendency is expected for $[(TMPyP^+)M]^{\bullet-}/[SWCNT]^{\bullet+}$.

Fluorescence Measurements. The formations of $(TMPyP^+)M$/ssDNA and $(TMPyP^+)M$/ssDNA/SWCNT(n,m) can also be confirmed by the fluorescence quenching measurements of $(TMPyP^+)M$, which also give information about the relaxation rates via $^1[(TMPyP^+)M]^*$ in the hybrids.[29] Steady-state fluorescence spectral changes of $(TMPyP^+)Zn$ on addition of ssDNA in H_2O (λ_{ex} = 435 nm) are shown in Figure 6. The original intensities of the fluorescence peaks of $(TMPyP^+)Zn$ located at 630 and 670 nm (shoulder) decrease until about 60% on addition of excess ssDNA, which gives additional evidence for the complex formation and occurrence of the CS-2 process. A similar phenomenon was also observed for $(TMPyP^+)H_2$; the fluorescence bands in the 650−750 nm region are quenched until about 50% on addition of excess ssDNA (see Figure S6, Supporting Information). It may be mentioned here that such fluorescence quenching of $(TMPyP^+)M$ was not observed by addition of poly(dA-dT) (lacking guanidine electron donor entities),[30] suggesting that the quenching of $(TMPyP^+)M$ by ssDNA is not due to a simple hydrogen bonding stacking effect but perhaps due to electron transfer. As discussed in the subsequent sections, dynamic quenching was found by the fluorescence lifetime shortening, denying that the quenching was only due to the ground state interactions but supporting the events via $^1[(TMPyP^+)M]^*$.[31] Additionally, an electron transfer from

^{1}(TMPyP$^+$)M* to ssDNA can be predominantly considered, but not the EnT process, since the excited singlet states of the DNA bases are all higher than that of ^{1}(TMPyP$^+$)M*.

Figure 7 shows further quenching of the steady-state fluorescence intensity of (TMPyP$^+$)Zn (over 80−90% of the original intensity) upon increasing the concentration of ssDNA/SWCNT(6,5) and ssDNA/SWCNT(7,6) in H_2O (λ_{ex} = 435 nm), supporting the formation of bionano hybrids, (TMPyP$^+$)Zn/ssDNA/SWCNT-(*n*,*m*). Although the occurrence of both CS process and EnT process from the ^{1}[(TMPyP$^+$)Zn]* to SWCNT(*n*,*m*) over ssDNA could be envisioned, the CS process is favorable in highly polar aqueous solution. In addition, the negligible spectral overlap between the (TMPyP$^+$)Zn fluorescence and the SWCNT-(*n*,*m*) absorption makes the EnT quenching process less likely based on the Förster theory.[26a]

The ssDNA/SWCNT(7,6) quenches the (TMPyP$^+$)Zn fluorescence intensity (Figure 7b) more efficiently than ssDNA/SWCNT(6,5) (Figure 7a). A similar tendency of the fluorescence quenching was also observed for (TMPyP$^+$)H_2 on addition of ssDNA/SWCNT(*n*,*m*) (see Supporting Information; Figure S6).

To obtain the decay kinetic data of ^{1}[(TMPyP$^+$)M]* in the donor−acceptor nanohybrids, the picosecond time-resolved fluorescence measurements were performed with streak-scope method. Figure 8 shows the fluorescence time profiles of pristine (TMPyP$^+$)M, giving the lifetimes as $(\tau_F)_{ref}$ = 1250 ps for (TMPyP$^+$)Zn (Figure 8(a)) and 4010 ps for (TMPyP$^+$)H_2 (Figure 8(b)). Addition of ssDNA moderately accelerated the fluorescence decays, which could be curve-fitted to a biexponential decay function, giving the lifetimes ($(\tau_F)_{MP/DNA}$) to be 750 ps for (TMPyP$^+$)Zn and 950 ps for (TMPyP$^+$)H_2 with

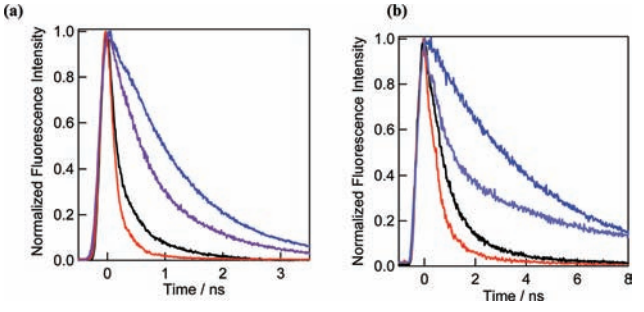

Figure 8. Fluorescence decays of (a) (TMPyP$^+$)Zn and (b) (TMPyP$^+$)H_2 in H_2O (λ_{ex} = 408 nm). Blue line for (TMPyP$^+$)M, violet line for addition of ssDNA, black line for addition of ssDNA/SWCNT(6,5), red line for addition of ssDNA/SWCNT(7,6). Excess ssDNA and ssDNA/SWCNT(*n*,*m*) are added until the decays are saturated.

major short components (fraction (Fr) > 60%); the remaining minor longer components are due to the noninteracting porphyrin entities. Furthermore, additions of ssDNA/SWCNT(6,5) and ssDNA/SWCNT(7,6) to (TMPyP$^+$)M drastically accelerated the fluorescence decays of (TMPyP$^+$)M, in agreement with the steady-state fluorescence intensity quenching in Figure 7. The curve fittings of these fluorescence time profiles with a biexponential decay function gave the major short component ($(\tau_F)_{MP/DNA/CNT}$ = 200−500 ps, Fr = 80−90%) as summarized in Table 2 and the remaining minor longer component attributable to the noninteracting porphyrin entities. The $(\tau_F)_{ZnP/DNA/CNT}$ values for (TMPyP$^+$)Zn/ssDNA/SWCNT(*n*,*m*) were found to be 170−210 ps, which are shorter than $(\tau_F)_{H2P/DNA/CNT}$ (420−540 ps) for (TMPyP$^+$)H_2/ssDNA/SWCNT(*n*,*m*). In each (TMPyP$^+$)M, SWCNT(7,6) gives a shorter $(\tau_F)_{ZnP/DNA/CNT}$ value than that of SWCNT(6,5).

The difference in shortening of the fluorescence lifetimes on addition of ssDNA is mainly ascribed to the CS-2 process since EnT from ^{1}[(TMPyP$^+$)M]* to ssDNA is energetically unfavorable; furthermore, fluorescence lifetime shortening due to a hydrogen bonding stacking effect was not observed in the presence of poly(dA-dT).[30] Thus, the rate constant for the CS-2 process (k_{CS-2}) can be evaluated from the difference between $1/(\tau_F)_{MP/DNA}$ and $1/(\tau_F)_{ref}$ as $((0.5 - 0.6) \times 10^9\ s^{-1})$ in Table 2; these k_{CS-2} values are almost one order smaller compared to those of the sufficiently exothermic CS processes,[11] although these k_{CS-2} values do not reflect the ΔG_{CS-2} values (slightly exothermic for (TMPyP$^+$)H_2 and endothermic for (TMPyP$^+$)Zn) based on rough estimations.

The overall fluorescence quenching rates (k_q) are calculated from the differences between $1/(\tau_F)_{MP/DNA/CNT}$ for (TMPyP$^+$)M/ssDNA/SWCNT(*n*,*m*) and $1/(\tau_F)_{ref}$ for (TMPyP$^+$)M;[29] the k_q values contain the rate constants of the CS-1 process (k_{CS-1}) and EnT process (k_{EnT}) in addition to k_{CS-2} values. As proved in the previous section for the fluorescence intensity quenching, the contribution of k_{EnT} may be negligibly small; therefore, k_{CS-1} can be evaluated as $k_{CS-1} \approx k_q - k_{CS-2}$.[20] As listed in Table 2, the evaluated k_{CS-1} values are in the range of $(1.5-4.5) \times 10^9\ s^{-1}$, which are reasonable values as the CS-1 process via ^{1}(TMPyP$^+$)M* vs SWCNT(*n*,*m*) with a separation distance of ~6 Å.[19] The Φ_{CS-1} and Φ_{CS-2} values evaluated in a usual manner shown in Table 2 are larger than 0.83 and 0.35, respectively; even considering the fraction of the short fluorescence lifetimes, which correspond to the fraction of the complexes, they are larger than 0.71 and 0.35, respectively.

For (TMPyP$^+$)M/ssDNA/SWCNT(*n*,*m*), a comparison of k_{CS-1} between (TMPyP$^+$)Zn and (TMPyP$^+$)H_2 reveals the tendency that (TMPyP$^+$)Zn is a better electron donor than

Table 2. Fluorescence Lifetimes (τ_F) and Fractions (Fr) of Fast Decay Component, Rate Constants of Charge Separations (k_{CS}) and Total Quenching (k_q), and Quantum Yields (Φ_{CS}) of (TMPyP$^+$)M in Nanohybrids in H_2O

nanohybrids	τ_F/ps (Fr)	k_{CS-2}/s^{-1}[a]	k_q/s^{-1}[b]	k_{CS-1}/s^{-1}[c]	Φ_{CS}[a] (× Fr)
(TMPyP$^+$)Zn/ssDNA	750 (100%)	0.5×10^9	--	--	0.35 (0.35)[d]
(TMPyP$^+$)Zn/ssDNA/SWCNT(6,5)	210 (85%)	--	3.9×10^9	3.4×10^9	0.83 (0.71)[e]
(TMPyP$^+$)Zn/ssDNA/SWCNT(7,6)	170 (90%)	--	5.0×10^9	4.5×10^9	0.86 (0.77)[e]
(TMPyP$^+$)H_2/ssDNA	950 (60%)	0.6×10^9	--	--	0.76 (0.46)[d]
(TMPyP$^+$)H_2/ssDNA/SWCNT(6,5)	540 (87%)	--	2.1×10^9	1.5×10^9	0.89 (0.77)[e]
(TMPyP$^+$)H_2/ssDNA/SWCNT(7,6)	420 (92%)	--	2.6×10^9	2.0×10^9	0.97 (0.89)[e]

[a] For (TMPyP$^+$)M/ssDNA, $k_{CS-2} = (1/\tau_f)_{MP/DNA} - (1/\tau_f)_{ref}$ and $\Phi_{CS-2} = [(1/\tau_f)_{MP/DNA} - (1/\tau_f)_{ref}]/(1/\tau_f)_{MP/DNA}$. Here, $(\tau_f)_{ref}$ = 1250 ps for (TMPyP$^+$)Zn and 4010 ps for (TMPyP$^+$)H_2. [b] For (TMPyP$^+$)M/ssDNA/SWCNT(*n*,*m*), $k_q = \{(1/\tau_f)_{MP/DNA/CNT} - (1/\tau_f)_{ref}\}$ and $\Phi_q = \{(1/\tau_f)_{MP/DNA/CNT} - (1/\tau_f)_{ref}\}/(1/\tau_f)_{MP/DNA/CNT}$.[29] [c] $k_{CS-1} = k_q - k_{CS-2}$, $\Phi_{CS-1} = \Phi_q - \Phi_{CS-2}$. [d] For the CS-2 process. [e] For the CS-1 process.

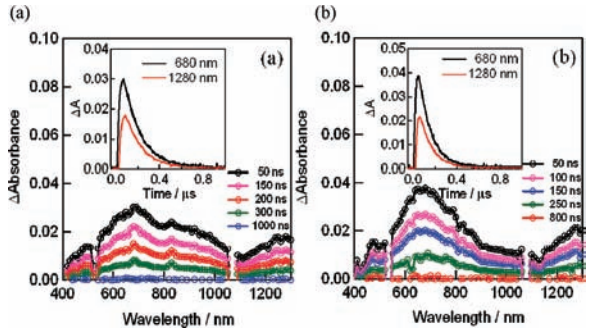

Figure 9. Nanosecond transient absorption spectra of $(TMPyP^+)Zn$/ssDNA/SWCNT(n,m) observed by 532 nm laser-light irradiation (ca. 3 mJ/pulse) in Ar-saturated H_2O. (a) SWCNT(6,5) and (b) SWCNT(7,6). Spikes at 532 and 1064 nm are due to scattering light from the YAG laser. Inset: time profile at 680 and 1280 nm.

$(TMPyP^+)H_2$, which follows the order of the $\Delta G_{CS\text{-}1}$ values listed in Table 1. For each $(TMPyP^+)M$, the $k_{CS\text{-}1}$ and $\Phi_{CS\text{-}1}$ values for SWCNT(7,6) are slightly larger than those for SWCNT(6,5), although the $\Delta G_{CS\text{-}1}$ values do not follow this order, suggesting that other factors such as size of SWCNT(n,m) may affect the $k_{CS\text{-}1}$ values. For the EM process, the fluorescence data unfortunately cannot give any information.

Nanosecond Transient Absorption Studies. Evidence for the CS processes can be obtained from the transient absorption spectral studies by the observation of the radical ions as intermediate products; furthermore, their decays can afford the rate constant of the CR process, k_{CR}, between the radical ions. Figure 9 shows the nanosecond transient absorption spectra of the $(TMPyP^+)Zn$/ssDNA/SWCNT(n,m) nanohybrids observed using a 532 nm laser light, which predominantly excites the $(TMPyP^+)Zn$ moiety. A transient absorption peak corresponding to the formation of $[(TMPyP^+)Zn]^{\bullet+}$ appears around 660 nm.[20] As the counterpart of the $[(TMPyP^+)Zn]^{\bullet+}$ unit, $[SWCNT]^{\bullet-}$ would be anticipated to form. Indeed, the broad absorption bands that appeared in the 1250−1300 nm range can be assigned to $[SWCNT(n,m)]^{\bullet-}$.[19] The absorption intensities in the visible and NIR region decay in similar time intervals, suggesting that $[(TMPyP^+)Zn]^{\bullet+}$ is coupled to $[SWCNT]^{\bullet-}$. Compared with $(TMPyP^+)Zn$/ssDNA/SWCNT-(6,5) in Figure 9a, the transient absorption bands in the 800−1000 nm region and 1250−1300 nm region for the SWCNT(7,6) analogue in Figure 9b are sharp and intense. The transient band near 1000 nm is intense for $(TMPyP^+)Zn$/ssDNA/SWCNT(6,5), suggesting that $[SWCNT(6,5)]^{\bullet-}$ has an additional absorption band near 1000 nm in addition to the broad band around 1280 nm.

In the time profiles at 680 and 1280 nm shown in the insets of Figure 9, the rises of the $[(TMPyP^+)Zn]^{\bullet+}$ were found to be fast within the nanosecond laser-light pulse (6 ns), which may correspond to the $k_{CS\text{-}1}$ ($>10^9$ s^{-1}) as estimated from the fluorescence lifetimes (Table 2). After reaching a maximum immediately after the laser-light irradiation, the absorption intensities of $[(TMPyP^+)Zn]^{\bullet+}$ begin to decay within about 1000 ns. From the first-order fitting of the decay curves at 680 and 1280 nm, almost the same CR rate constants (k_{CR}) of $[(TMPyP^+)Zn]^{\bullet+}$/ssDNA/$[SWCNT(n,m)]^{\bullet-}$ were evaluated: 6.8×10^6 s^{-1} and 8.1×10^6 s^{-1} for SWCNT(6,5) and SWCNT(7,6), respectively, as listed in Table 3. Using the k_{CR} values, the lifetimes of RIPs, τ_{RIP} (= $1/k_{CR}$), were evaluated to be 160 and 120 ns, respectively, indicating that the RIP for SWCNT(6,5) persists for slightly longer than that for SWCNT(7,6).

Table 3. Rate Constants of Charge Recombination (k_{CR}) and Lifetimes of the Radical Ion Pair (τ_{RIP}) and Ratios (k_{CS}/k_{CR}) in H_2O

nanohybrids	k_{CR}/s^{-1}	τ_{RIP}/ns	k_{CS}/k_{CR}
$(TMPyP^+)Zn$/ssDNA/SWCNT(6,5)	6.4×10^{6a}	160	540
$(TMPyP^+)Zn$/ssDNA/SWCNT(7,6)	8.1×10^{6a}	120	470
$(TMPyP^+)H_2$/ssDNA/SWCNT(6,5)	4.6×10^{6b}	220	320
$(TMPyP^+)H_2$/ssDNA/SWCNT(7,6)	6.4×10^{6b}	160	310

[a] k_{CR} evaluated from 1280 nm $(TMPyP^+)Zn$/ssDNA/SWCNT(n,m); 6.6×10^6 s^{-1} for SWCNT(6,5) and 8.5×10^6 s^{-1} for SWCNT(7,6). [b] k_{CR} evaluated from 1280 nm $(TMPyP^+)H_2$/ssDNA/SWCNT(n,m); 4.4×10^6 s^{-1} for SWCNT(6,5) and 6.3×10^6 s^{-1} for SWCNT(7,6).

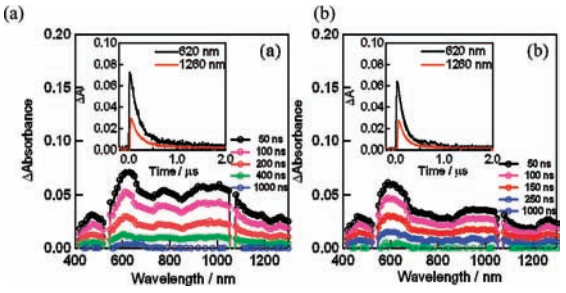

Figure 10. Nanosecond transient absorption spectra of $(TMPyP^+)H_2$/ssDNA/SWCNT(n,m) observed by 532 nm (ca. 3 mJ/pulse) laser irradiation in Ar-saturated H_2O: (a) SWCNT(6,5) and (b) SWCNT-(7,6). Spikes at 532 and 1064 nm are due to scattered light from the YAG laser. Inset: Time profiles at 620 and 1260 nm.

Figure 10 shows the nanosecond transient absorption spectra of $(TMPyP^+)H_2$/ssDNA/SWCNT(n,m) nanohybrids. The relatively sharp band at 620 nm is assigned to $[(TMPyP^+)H_2]^{\bullet+}$, and the NIR bands around 1250−1300 nm are assigned to $[SWCNT(n,m)]^{\bullet-}$. The absorption band near 1000 nm stands out because of the sharpness and blue-shift of the $[(TMPyP^+)H_2]^{\bullet+}$ absorption bands which extend to the longer wavelength region deform the NIR bands. The absorption intensities homogeneously decrease with time intervals in the whole region, suggesting that the species in the visible region are paired with the species in the NIR region. Compared with SWCNT(7,6) in Figure 10b, the absorption bands for SWCNT(6,5) in Figure 10a show intense absorptions near 800 and 1000 nm, suggesting that $[SWCNT(6,5)]^{\bullet-}$ has such absorptions near here, too. Similar spectral characteristics can be found for $(TMPyP^+)Zn$/ssDNA/SWCNT(6,5) as shown in Figure 9b, compared with SWCNT(7,6)-analogy in Figure 9b.

The CS-2 process would anticipate the formation of $[(TMPyP^+)M]^{\bullet-}$ and $[ssDNA]^{\bullet+}$, which are tracked by the EM process finally generating $[(TMPyP^+)M]^{\bullet-}$ and $[SWCNT]^{\bullet+}$. The absorption peaks of the porphyrin radical anions were recently reported to appear in the 650−700 nm spectral range.[32] The absorption bands of $[SWCNT]^{\bullet+}$ have also been reported to appear in the NIR region similar to $[(TMPyP^+)Zn]^{\bullet-}$.[20] Although a 500 nm transient band is anticipated for $ssDNA^{\bullet+}$ (mainly guanidine cation),[33] it was difficult to assign this band solely to $ssDNA^{\bullet+}$ since the triplet states of $(TMPyP^+)M$ also showed the characteristic band near 500 nm (see Figures S7 and S8 in Supporting Information). Furthermore, the hole of $ssDNA^{\bullet+}$ might shift to SWCNT or might charge recombine with $[(TMPyP^+)M]^{\bullet-}$, resulting in a quick disappearance of the $ssDNA^{\bullet+}$ band. Therefore, although the CS-2/EM process is a possible process, it remains to be proven.

From the decays of the 620 and 1260 nm bands, the k_{CR} values of $[(TMPyP^+)H_2]^{\bullet+}$/ssDNA/$[SWCNT(n,m)]^{\bullet-}$ were evaluated to be 4.6×10^6 and 6.4×10^6 s^{-1}, which correspond to τ_{RIP} with 220 and 160 ns for SWCNT(6,5) and SWCNT(7,6), respectively (Table 3). For each SWCNT(n,m), the RIP for $(TMPyP^+)H_2$ persists for a longer time than that for $(TMPyP^+)$Zn, which is the reverse order of the $E_{RIP(CS-1)}$ values ($(TMPyP^+)H_2 \gg (TMPyP^+)$Zn), suggesting that the CR process may belong to the inverted region of the Marcus plot;[28] that is, this consideration suggests that the main process for $(TMPyP^+)$Zn/ssDNA/SWCNT-(n,m) is CS-1 rather than the CS-2/EM process. On the other hand, the observation of slightly longer τ_{RIP} values for SWCNT(6,5) than those for SWCNT(7,6) may be difficult to predict because of the small difference in $E_{RIP(CS-1)}$ values ($\approx$0.04 eV). These τ_{RIP} values are slightly longer than the earlier reported values for $(TMPyP^+)$M/$^-$OOC-pyrene/SWCNT(n,m),[19] suggesting that arrangements of $(TMPyP^+)$M with respect to SWCNTs over ssDNA are appropriate for longer persistence of the RIPs, in which the ssDNA acts as a separating agent of the opposite charges.

Table 3 also lists the ratio of k_{CS}/k_{CR} as a kinetic measure of the charge accumulation for utilization of the electron−hole pair in the nanohybrids under light illumination, which is usually termed as "charge-stabilization ability".[34,35] The k_{CS}/k_{CR} ratios for $(TMPyP^+)$Zn/ssDNA/SWCNT(n,m) are larger than those for $(TMPyP^+)H_2$/ssDNA/SWCNT(n,m) by a factor of ca. 1.5, suggesting a higher "charge-stabilization ability" for $(TMPyP^+)$Zn nanohybrids.[20] For each porphyrin, the k_{CS}/k_{CR} ratios for SWCNT-(6,7) are larger than those of SWCNT(7,6), suggesting slightly higher charge-stabilization ability of SWCNT(6,5) nanohybrids.

CONCLUSIONS

We have successfully built bionano donor−acceptor hybrids, $(TMPyP^+)$M/ssDNA/SWCNT(n,m), capable of undergoing photoinduced electron transfer in H_2O. As confirmed by the fluorescence quenching measurements and transient absorption measurements, a photoinduced charge-separation process occurs via the excited singlet state of the $(TMPyP^+)$M moiety to SWCNTs overshooting the wrapped ssDNA, producing the radical ion pairs, $[(TMPyP^+)M]^{\bullet+}$/ssDNA/$[SWCNT(n,m)]^{\bullet-}$. In this case, ssDNA acts as glue between $(TMPyP^+)$M and SWCNT(n,m)s. When ssDNA is capable of donating electron to the excited singlet state of $(TMPyP^+)$M, $[(TMPyP^+)M]^{\bullet-}$/$[ssDNA]^{\bullet+}$/SWCNT-(n,m) is formed, which is followed by the electron migration from SWCNT(n,m) to ssDNA$^{\bullet+}$, finally producing $[(TMPyP^+)M]^{\bullet-}$/ssDNA/$[SWCNT(n,m)]^{\bullet+}$. In this case, ssDNA acts as an electron donor and a electron-migrating agent. For both cases, appreciable differences are recognized between $(TMPyP^+)$Zn and $(TMPyP^+)H_2$; that is, the former having higher charge-stabilization ability. Thus, higher photocurrents in the photoelectrochemical solar cells constructed using supramolecular assemblies of $(TMPyP^+)$Zn/ssDNA/SWCNT hybrids would be expected compared with the $(TMPyP^+)H_2$ analogies. Further studies along this line are in progress.

EXPERIMENTAL SECTION

Chemicals. The (6,5)- and (7,6)-enriched SWCNTs were produced by CoMoCAT, SouthWest Nano Technologies, Inc. (Norman, OK),[18] marketed by Aldrich Chemicals (Milwaukee, WI). Calf thymus ssDNA was from Sigma-Aldrich. The water-soluble tetrakis(4-*N*-methylpyridyl)porphyrin ($(TMPyP^+)$M; M = Zn and H_2) was purchased from Midwest Chemicals, Chicago (IL), and purified over a sephadex LH20 column prior to use.

Preparation of $(TMPyP^+)$M/ssDNA/SWCNT(n,m) Nanohybrids. A known amount of ssDNA was dissolved in Millipore water at 0−5 °C. The concentration of ssDNA was determined by absorbance at 260 nm ($\varepsilon_{260\ nm} = 6.6 \times 10^3\ M^{-1}\ cm^{-1}$).[36] The stock solution so prepared was used to solubilize SWCNTs. For preparation of ssDNA/SWCNT(n,m), to a solution of ssDNA, SWCNT(7,6) or SWCNT(6,5) (0.5−1.0 mg) was added and sonicated for 20 min. The resultant solution was then centrifuged for 30 min at 3000 rpm. The supernatants were, then, separated from the bundles that were settled at the bottom of the centrifuged tube. By doing so, we have been able to obtain highly solubilized ssDNA/SWCNT(6,5) and ssDNA/SWCNT(7,6) hybrids in solution that was stored below 4 °C for further studies. The nanotube solution thus obtained was very stable for a number of days as proven by the absorption and emission data. To form references, $(TMPyP^+)$M/ssDNA, $(TMPyP^+)$M of known concentration was dissolved in Millipore water, to which a known amount of ssDNA aqueous solution was added. To form $(TMPyP^+)$M/ssDNA/SWCNT-(n,m) nanohybrids, a known amount of $(TMPyP^+)$M aqueous solution was added to ssDNA/SWCNT(n,m).

For spectroscopic titration measurements of two-layered nanohybrids, a small aliquot (in microliter volume) of ssDNA was added to an aqueous solution of $(TMPyP^+)$M. For the preparation of three-layered nanohybrids, a small aliquot (in microliter volume) of ssDNA/SWCNT-(n,m) was added to $(TMPyP^+)$M; this procedure tends to prevent the direct adsorption of $(TMPyP^+)$M on SWCNT(n,m).

Instrumentations. The UV−visible−NIR spectral measurements were carried out with a Perkin-Elmer (Lamda 750) or Jasco V-670 spectrophotometer. The steady-state fluorescence spectra were monitored by using a Perkin-Elmer (LS-55) or a Horiba Jobin Yvon Nanolog UV−visible−NIR spectrofluorometer equipped with PMT (for UV−visible) and InGaAs (for NIR) detectors. All the solutions were purged prior to spectral measurements using nitrogen gas.

Transmission electron micrograph (TEM) measurements were recorded by applying a drop of the sample to a copper grid and after drying the solvent. Images were recorded on a Hitachi H-7650 transmission electron microscope at an accelerating voltage of 120 kV for imaging.

The time-resolved fluorescence spectra were measured by a single photon counting method using a streak scope (Hamamatsu Photonics, C5680) as a detector and a laser light (Hamamatsu Photonics M10306, laser diode head, 408 nm) as an excitation source. Lifetimes were evaluated with software attached to the equipment.

Nanosecond transient absorption measurements were carried out using SHG (532 nm, 5−6 ns pulse width) of a Nd:YAG laser (Spectra-Physics, Quanta-Ray GCR-130, 5 ns fwhm) as an excitation source. For transient absorption spectra in the NIR region (600−1200 nm) and the time profiles, monitoring the light from a pulsed Xe lamp was detected with a Ge-APD (Hamamatsu Photonics, B2834). For the measurements in the visible region (400−1000 nm), a Si-PIN photodiode (Hamamatsu Photonics, S1722−02) was used as a detector.

The computational calculations were performed by PM3 methods with the GAUSSIAN 03 software package[37] on high speed computers.

ASSOCIATED CONTENT

Supporting Information. TEM images, TEM histograms, and optical absorption and emission spectra of selected bionano hybrids, energy level diagram showing the photochemical events in the nanohybrids, transient absorption spectra of $(TMPyP^+)$M/ssDNA, and complete citation for ref 37. This material is available free of charge via the Internet at http://pubs.acs.org.

AUTHOR INFORMATION

Corresponding Author
francis.dsouza@unt.edu; ito@tagen.tohoku.ac.jp

■ ACKNOWLEDGMENT

This work was financially supported by the National Science Foundation (Grant Nos. 0804015 and CHE-1110942 to FD). We thank Prof. H. Murata of JAIST for his support.

■ REFERENCES

(1) Saenger, W. *Principles of Nucleic Acid Structure*; Springer-Verlag: New York, 1984.

(2) (a) Iijima, S. *Nature* **1991**, *354*, 56–58. (b) Iijima, S.; Ichihashi, T. *Nature* **1993**, *364*, 603–605.

(3) (a) Harris, P. J. F. *Carbon Nanotubes and Related Structures: New Materials for the Twenty-First Century*; Cambridge University Press: Cambridge, UK, 2001. (b) Dresselhaus, M. S., Dresselhaus, G., Avouris, P., Eds. *Carbon Nanotubes: Synthesis, Structure and Applications*; Springer Publishing: New York, 2001.

(4) (a) *Handbook of Carbon Nano Materials*; D'Souza, F., Kadish, K. M., Eds.; World Scientific: Singapore, 2011. (b) Reich, S.; Thomsen, C.; Maultzsch, J. *Carbon Nanotubes: Basic Concepts and Physical Properties*; Wiley-VCH: Weinheim, 2004. (c) Roth, S.; Carroll, D. *One-Dimensional Metals: Conjugated Polymers, Organic Crystals, Carbon Nanotubes*; Wiley-VCH: Weinheim; Germany, 2004. (d) Meyyappan, M. *Carbon Nanotubes, Science and Application*; Wiley-VCH: Weinheim, Germany, 2006. (e) Saito, R.; Dresselhaus, G.; Dresselhaus, M. D. *Physical Properties of Carbon Nanotubes*; Imperial College Press: London, 1998.

(5) (a) Staii, C.; Chen, M.; Gelperin, A.; Johnson, A. T. *Nano Lett.* **2005**, *5*, 1774–1778. (b) Jeng, E. S.; Moll, A. E.; Roy, A. C.; Gastala, J. B.; Strano, M. S. *Nano Lett.* **2006**, *6*, 371–375.(c) Rotkin, S. V. In *Handbook of Carbon Nano Materials*; D'Souza, F., Kadish, K. M., Eds.; World Scientific: Singapore, 2011; Chapter 23, Vol. 2, pp 787−823.

(6) (a) Zheng, M.; Jagota, A.; Semke, E. D.; Diner, B. A.; McLean, R. S.; Lustig, S. R.; Richardson, R. E.; Tassi, N. G. *Nat. Mater.* **2003**, *2*, 338–342. (b) Zheng, M.; Jagota, A.; Strano, M. S.; Santos, A. P.; Barone, P.; Chou, S. G.; Diner, B. A.; Dresselhaus, M. S.; McLean, R. S.; Onoa, G. B.; Samsonidze, G. G.; Semke, E. D.; Usrey, M.; Walls, D. J. *Science* **2003**, *302*, 1545–1548.

(7) Meng, S.; Maragakis, P.; Papaloukas, C.; Kaxiras, E. *Nano Lett.* **2007**, *7*, 45–50.

(8) (a) Sgobba, V.; Rahman, G. M. A.; Guldi, D. M. In *Carbon Nanotubes in Electron Donor−Acceptor Nanocomposites, Chemistry of Carbon Nanotubes*; Basiuk, V. A., Ed.; American Scientific Publishers: USA, 2006. (b) Sgobba, V.; Rahman, G. M. A.; Ehli, C.; Guldi, D. M. In *Fullerenes-Principles and Applications*; Langa, F., Nierengarten, N. J., Eds.; Royal Society of Chemistry: Cambridge, UK, 2007. (c) Sgobba, V.; Guldi, D. M. *Chem. Soc. Rev.* **2009**, *38*, 165–184.

(9) (a) Delgado, J. L.; Herranz, M. Á.; Martín, N. *J. Mater. Chem.* **2008**, *18*, 1417–1426.(b) Bottair, G.; de la Torre, G.; Guldi, D. M.; Torres, T. *Chem. Rev.* 2010, *110*, 6768.(c) Tasis, D.; Tagmatarchis, N.; Bianco, A.; Prato, M. *Chem. Rev.* **2006**, *106*, 1105.

(10) Fukuzumi, S.; Kojima, T. *J. Mater. Chem.* **2008**, *18*, 1427–1439.

(11) (a) D'Souza, F.; Ito, O. *Chem. Soc. Rev.* DOI: 10.1039/c1cs15201g, in press. (b) D'Souza, F.; Ito, O. In *Handbook of Porphyrin Science*; Kadish, K. M., Guilard, R., Smith, K. M., Eds.; World Science Publishers: Singapore, 2010; Vol. 1, Chapter 4, pp 307−437. (c) D'Souza, F.; Ito, O. *Chem. Commun.* **2009**, *45*, 4913–4928.

(12) Tanaka, Y.; Hirana, Y.; Niidome, Y.; Kato, K.; Saito, S.; Nakashima, N. *Angew. Chem., Int. Ed.* **2009**, *48*, 7655–7659.

(13) (a) Zheng, M.; Jagota, A.; Strano, M. S.; Santos, A. P.; Barone, P.; Chou, S. G.; Diner, B. A.; Dresselhaus, M. S.; McLean, R. S.; Onoa, G. B.; Samsonidze, G. G.; Semke, E. D.; Usrey, M.; Walls, D. J. *Science* **2003**, *302*, 1545–1548. (b) Meng, S.; Maragakis, P.; Papaloukas, C.; Kaxiras, E. *Nano Lett.* **2007**, *7*, 45–50. (c) Campbell, J. F.; Tessmer, I.; Thorp, H. H.; Erie, D. A. *J. Am. Chem. Soc.* **2008**, *130*, 10648–10655.

(14) (a) Dukovic, G.; Balaz, M.; Doak, P.; Berova, N. D.; Zheng, M.; McLean, R. S.; Brus, L. E. *J. Am. Chem. Soc.* **2006**, *128*, 9004–9005. (b) Hughes, M. E.; Brandin, E.; Golovchenko, J. A. *Nano Lett.* **2007**, *7*, 1191–1194.

(15) (a) Johnson, R. R.; Johnson, A. T. C.; Klein, M. L. *Nano Lett.* **2008**, *8*, 69–75. (b) Manohar, S.; Tang, T.; Jagota, A. *J. Phys. Chem. C* **2007**, *111*, 17835–17845. (c) Johnson, R. R.; Kohlmeyer, A.; Johnson, A. T. C.; Klein, M. L. *Nano Lett.* **2009**, *9*, 537–541. (d) Gao, H.; Kong, Y. *Ann. Rev. Mater. Res.* **2004**, *34*, 123–150.

(16) *The Porphyrin Handbook*; Kadish, K. M., Smith, K. M., Guilard, R., Ed.; Academic Press: San Diego, 2000; Vol. 9.

(17) (a) Herrera, J. E.; Resasco, D. E. *Chem. Phys. Lett.* **2003**, *376*, 302–309. (b) Herrera, J. E.; Pompeo, B. F.; Resasco, D. E. *J. Nanosci. Nanotechnol.* **2003**, *3*, 133–138. (c) Jorio, A.; Santos, A. P.; Ribeiro, H. B.; Fantini, C.; Souza, M.; Vieira, J. P. M.; Furtado, C. A.; Jiang, J.; Saito, R.; Balzano, L.; Resasco, D. E.; Pimenta, M. A. *Phys. Rev. B* **2005**, *72*, 075207/1–075207/5. (d) Hennrich, F.; Krupke, R.; Lebedkin, S.; Arnold, K.; Fischer, R.; Resasco, D. E.; Kappes, M. M. *J. Phys. Chem. B* **2005**, *109*, 10567–10573.

(18) Also see manufacturer's website http://swentnano.com/ for additional product details.

(19) See for procedural details: Das, S. K.; Subbaiyan, N. K.; D'Souza, F.; Sandanayaka, A. S. D.; Hasobe, T.; Ito, O. *Energy Environ. Sci.* **2011**, *4*, 707–716.

(20) (a) Maligaspe, E.; Sandanayaka, A. S. D.; Hasobe, T.; Ito, O.; D'Souza, F. *J. Am. Chem. Soc.* **2010**, *132*, 8158–8164. (b) Sandanayaka, A. S. D.; Maligaspe, E.; Hasobe, T.; Ito, O.; D'Souza, F. *Chem. Commun.* **2010**, *46*, 8749–8751. (c) Sandanayaka, A. S. D.; Subbaiyan, N. K.; Das, S. K.; Chitta, R.; Maligaspe, E.; Hasobe, T.; Ito, O.; D'Souza, F. *ChemPhysChem* **2011**, *12*, 2266–2273.

(21) (a) Weisman, R. B.; Bachilo, S. M. *Nano Lett.* **2003**, *3*, 1235–1238. (b) Luo, Z.; Pfefferle, L. D.; Haller, G. L.; Papadimitrakopoulos, F. *J. Am. Chem. Soc.* **2006**, *128*, 15511–15516.

(22) Gao, H.; Kong, Y. *Ann. Rev. Mater. Res.* **2004**, *34*, 123–150.

(23) (a) Kavan, L.; Dunsch, L. *Electrochemistry of Carbon Nanotubes in Carbon Nanotubes: Advanced Topics in the Synthesis Structure, Properties and Applications*; Springer: Berlin, 2008; Vol. III. (b) Paolucci, D.; Franco, M. M.; Iurlo, M.; Marcaccio, M.; Prato, M.; Zerbetto, F.; Pénicaud, A.; Paolucci, F. *J. Am. Chem. Soc.* **2008**, *130*, 7393–7399. (c) Ehli, C.; Oelsner, C.; Guldi, D. M.; Mateo-Alonso, A.; Prato, M.; Schmidt, C.; Backes, C.; Hauke, F.; Hirsch, A. *Nat. Chem.* **2009**, *1*, 243–249.

(24) It was difficult to get reliable electrochemical data of $(TMPyP^+)M$ in aqueous solution due to strong adsorption of porphyrin on the electrode surface and the irreversible nature of the redox peaks; thus, we employed the redox potentials in polar organic solvents. For SWCNT(n, m), the reported redox potentials in DMF (ref 12) are used in the present study.

(25) (a) Oliveria Brett, A. M.; Dickulescu, V.; Pieclade, J. A. P. *Bioelectrochemistry* **2002**, *55*, 61–62. (b) Fukuzumi, S.; Miyao, H.; Ohkubo, K.; Suenobu, T. *J. Phys. Chem. A* **2005**, *109*, 3285–3294.

(26) (a) Förster, T. *Ann. Phys.* **1948**, *437*, 55–75. (b) Dexter, D. L. *J. Chem. Phys.* **1953**, *21*, 836–850.(c) Turro, N. J.; Ramamurty, V.; Scaiano, J. C. *Priciples of Molecular Photochemistry, An Itroduction*; University Science Book: CA, 2009.

(27) (a) Rehm, D.; Weller, A. *Isr. J. Chem.* **1970**, *8*, 259–171. (b) Mataga, N.; Miyasaka, H. In *Electron Transfer*; Jortner, J., Bixon, M., Eds.; John Wiley & Sons: New York, 1999; Part 2, pp 431−496.

(28) (a) Marcus, R. A.; Sutin, N. *Biochim. Biophys. Acta* **1985**, *811*, 265–322. (b) Marcus, R. A. *Angew. Chem., Int. Ed. Engl.* **1993**, *32*, 1111–1121.

(29) Lakowicz, J. R. *Principles of Fluorescence Spectroscopy*, 3rd ed.; Springer: New York, 2006.

(30) D'Souza, F.; Rogers, L. M.; Islam, S; Araki, Y.; Ito, O.; Wada, T. *Chem. Lett.* **2008**, *37*, 460–461.

(31) Although it is expected that the fluorescence intensity of $(TMPyP^+)M$ decreases on addition of ssDNA due to the absorbance decrease by the ground-state interactions and dilution effect (Figure S4, Supporting Information), the observed shortening in the fluorescence lifetime supports that the fluorescence intensity quenching is mostly dynamic in nature.

(32) Kubo, M.; Mori, Y.; Otani, M.; Murakami, M.; Ishibashi, Y.; Yasuda, M.; Hosozumi, K.; Miyasaka, H.; Imahori, H.; Nakashima, S. *J. Phys. Chem. A* **2007**, *111*, 5136–5143.

(33) (a) Simon, J. D.; Peter, K. S. *J. Am. Chem. Soc.* **1982**, *104*, 6142–6144. (b) Ohkubo, K.; Yukimoto, K.; Fukuzumi, S. *Chem. Commun.* **2006**, 2504–2506.
(34) Sandanayaka, A. S. D.; Chitta, R.; Subbaiyan, N. K.; D'Souza, D.; Ito, O.; D'Souza, F. *J. Phys. Chem. C* **2009**, *113*, 13425–13432.
(35) D'Souza, F.; Sandanayaka, A. S. D.; Ito, O. *J. Phys. Chem. Lett.* **2010**, *1*, 2586–2590.
(36) Yellappa, S.; Seetharamappa, J.; Rogers, L. M.; Chitta, R.; Singhal, R. P.; D'Souza, F. *Bioconjugate Chem.* **2006**, *17*, 1418–1425.
(37) Frisch, M. J. et al. *Gaussian 03*; Gaussian, Inc.: Pittsburgh PA, 2003. See Supporting Information for complete details.